



## Size controlled copper nanoparticles hosted in mesoporous silica matrix: Preparation and characterization

Alessandro Gallo<sup>a,1</sup>, Tanya Tsoncheva<sup>b,\*</sup>, Marcello Marelli<sup>a</sup>, Mihail Mihaylov<sup>c</sup>, Momtchil Dimitrov<sup>b</sup>, Vladimiro Dal Santo<sup>a</sup>, Konstantin Hadjiivanov<sup>c</sup>

<sup>a</sup> Institute of Molecular Sciences and Technologies of the National Research Council, ISTM-CNR, Milano, Italy

<sup>b</sup> Institute of Organic Chemistry with Centre of Phytochemistry, Bulgarian Academy of Sciences, Sofia, Bulgaria

<sup>c</sup> Institute of General and Inorganic Chemistry, Bulgarian Academy of Sciences, Sofia, Bulgaria

### ARTICLE INFO

#### Article history:

Received 2 April 2012

Received in revised form 12 July 2012

Accepted 20 July 2012

Available online 27 July 2012

#### Keywords:

OMCVD technique

Copper nanoparticles supported on mesoporous silica

Methanol decomposition

Size dependent effects

FTIR spectroscopy

### ABSTRACT

A novel preparation strategy was performed to obtain uniform and size controlled, in a large scale, copper nanoparticles, hosted into mesoporous silica matrix. The method includes the initial deposition of finely dispersed copper nanoparticles, using a conventional incipient wetness impregnation of silica matrix with small amount of nitrate precursor and consecutive pretreatment in oxidation and reduction atmosphere. The further controlled growing of the loaded copper particles was performed in rotary bed reactor by step-wise deposition of copper over them by OMCVD techniques, using bis-(hexafluoroacetylacetone) copper (II) hydrate as a precursor. A complex of physicochemical methods (TEM, Nitrogen physisorption, TPR and TPRD-MS measurements, UV-Vis and FTIR spectroscopy of adsorbed CO) was used for characterization of the samples. The catalytic properties of the obtained materials were investigated in methanol decomposition to CO and hydrogen. A mechanism of the copper particles growing was discussed. Size dependent effects of the redox and catalytic properties of the loaded copper particles which are strongly affected by their location in the silica porous structure are assumed.

© 2012 Elsevier B.V. All rights reserved.

### 1. Introduction

The unique catalytic behaviour and the tunable optical, magnetic and electronic properties of metal nanoparticles have captured the attention of the research community and industry due to the potential application in many areas; electronics, sensing, transport, biomedicine, pharmacy, cosmetics, environmental analysis and remediation, catalysis and material sciences [1 and refs. therein]. Generally, these properties depend on the metal particle size [1]. Despite the steadily growing number of publications during the last two decades, most of them summarized in some valuable reviews [1–3], the controlled obtaining of nanostructured metal-containing samples still raises problems connected with the preparation, stabilization and characterization of small metal particles [1,3,4]. Another important problem is the determination of the critical particles size below which the typical metallic properties are lost [1,3,4].

Generally, the catalytic activity increases with the decrease of the particle size because of the increase of the fraction of the

surface-situated atoms. However, it is well documented that there are many reactions where the activity per surface atom (the so-called turn-over frequency, TOF) also depends on the particle size. These reactions are called structure-sensitive and examples are: enantioselective reactions, asymmetric hydrogenation, CO hydrogenation [1,5,6], aromatization of hexane [7], dehydration of diols [8], water gas shift reaction (WGSR) [9], ammonia synthesis [7,10], cyclopropane hydrogenolysis [11], light alkanes dehydrogenation [12,13], CO oxidation [14], Fischer-Tropsh reactions [15], autothermal reforming of hydrocarbon fuels to hydrogen [4,16,17], carbon deposition on metal particles [18], methane reforming [19], etc.

For very small particles increase of the energy level of valence electrons was proposed [1,4,20–24]. Alternatively, some authors assumed geometric origin of the size effect as a result of variations in the fraction of the face, step, edge and corner atoms [17,25,26]. It was found that the geometry of transition metal surface sites can have a pronounced impact on the dissociation of diatomic molecules containing  $\pi$ -bonds [27] and this process occurred over ensembles consisting of 5 or 6 metal atoms [19]. Hardeveld et al. [28] predicted that the number of these ensembles was maximal for metal nanoparticles in the range 1.8–2.5 nm. It was reported that the effect of structure sensitivity is connected with the crystal structures (planes, edges, corners) exposed to the reactants which determine the coordination number of active metal surface atoms

\* Corresponding author. Tel.: +359 9796640.

E-mail address: [tsoncheva@orgchm.bas.bg](mailto:tsoncheva@orgchm.bas.bg) (T. Tsoncheva).

<sup>1</sup> Present address: Department of Chemical Engineering, University of California, Santa Barbara, 93106-5080, USA.

and number of atoms in active ensembles. The change in the particle size can changes these parameters [11,29]. Obviously, for the supported nanoparticles, the elucidation of the size effects is complicated because (i) the contact with the support normally affects the crystal structure and the shape of the particles, (ii) the particles are only partially exposed to the reactants and (iii) additional electronic effects originating from the interaction of the particles with the support can occur.

Recently, methanol has been considered to be a new alternative of liquid fuels. It can be produced from natural gas, coal and number of renewable sources, such as black liquor, animal waste, biomass, etc. [30 and refs. therein]. On the other hand, methanol decomposition attracts growing interest due to the advantage of safe and efficient in situ production of hydrogen which can find application in gas turbines, fuel cells, vehicles and industry [31–49]. Moreover, the high endothermicity of methanol decomposition allows recovering the waste heat from vehicle exhausted gases and industrial processes. However, the various applications of this process need development of low cost, highly active and selective catalysts, working at relatively low temperatures. Transition metals and metal oxides have been intensively studied as good candidates of catalysts for methanol decomposition [50 and refs. therein] and supported metal nanoparticles have been found to demonstrate structure sensitivity [31,51–54]. Matsumura et al. [30] reported that silica supported nickel nanoparticles with size below 2–4 nm were less active than the larger ones. They related this feature to the poor crystallinity of smaller particles being in contact to the silica matrix, where weak adsorption of the reaction products (CO and H<sub>2</sub>) on pair nickel atoms was assumed [30,55]. We have recently reported that methanol decomposition on Ni/SiO<sub>2</sub> catalysts was characterized by structure sensitivity and TOF decreased with particle size increase in the range from 4 to 7 nm [56]. Croy et al. [31] also reported structure sensitivity of methanol decomposition on platinum nanoparticles ranging from 4 to 8 nm, the best performance being obtained for the smallest nanoparticles.

Copper containing catalysts are among the most active ones for many reactions as NO<sub>x</sub> and SO<sub>2</sub> reduction [57,58], dehydrogenation of methanol [59–62] and other alcohols [63–67], toluene combustion [68], WGSR [69], etc. It was reported that Cu nanoparticles dispersed on titania are active photocatalysts capable of operating under solar radiation for the production of hydrogen from ethanol and glycerol [70]. It was suggested that acetone hydrogenation over copper catalysts varied with particle size due to the altering of the adsorption behaviour of the reactants [71,72]. A particle size effect with magnesia-supported copper has been established in the dehydrogenation of 1-octanol to 1-octanal where increasing the particle size from 4.6 to 7.4 nm led to about 10% decrease in the yield of aldehyde [73]. It was demonstrated that the copper particles below 2–3 nm were completely inactive in 2-butanol dehydrogenation [54].

The controlled preparation of nanosized metal particles includes the choice of support as well as deposition technique. The most common method to stabilize highly dispersed metal particles is their deposition on high surface area inert support. The preparation method also affects the final properties of the particles in a great extent [1]. Co-precipitation, impregnation, ion exchange, decomposition of metallic cluster compounds, chemical deposition from colloids and metal vapor deposition are among the most frequently used approaches [1]. Organometallic Chemical Vapor Deposition (OMCVD) is a gas phase technique extensively used for the preparation of homogeneously dispersed nanosized supported catalysts [74,75]. OMCVD includes two steps, first adsorption of the precursor on the support surface followed by its decomposition [76–79]. OMCVD is often applied for deposition of metals, oxides, carbides and nitrides and offers many advantages in comparison to other methodologies. Photo-Fenton-like Cu/MCM-41 catalytic material

has been successfully prepared by OMCVD that demonstrated good activity in the degradation of Orange II in water [80]. Copper was also deposited in a similar way on a highly porous activated carbon from copper acetylacetone. A uniform deposition of copper onto the internal porous structure was detected by SEM-EDX technique [81]. The catalyst obtained showed superior catalytic activity in the wet oxidation of phenol as compared to the impregnated sample. Highly dispersed copper was also deposited through a cyclic two-step OMCVD process for preparation of Cu/ZnO/Al<sub>2</sub>O<sub>3</sub> catalysts. Their activity in methanol synthesis was higher as compared to that of a commercial catalyst [82]. The mild conditions, used for OMCVD, prevent deep synthering of the NPs, making the results easily reproducible [83]. This solvent free method is believed to increase the homogeneity of dispersion of nanoparticles (NPs).

The aim of the present study is to obtain information on the structure sensitivity of copper NPs hosted into mesoporous silica matrix with a high surface area in the methanol decomposition reaction. To this end, a novel stepwise method that combines the advantages of the incipient wetness impregnation and the OMCVD technique [84] was applied in order to produce size-controlled synthesis of materials with relative high copper loading and highly and homogeneously dispersed copper NPs. In order to obtain information on the structure sensitivity of supported copper particles, a complex of physicochemical methods, such as TEM, Nitrogen physisorption, TPR and TPRD-MS measurements, UV-Vis and FTIR spectroscopy of surface species as well as a catalytic decomposition of methanol to CO and hydrogen, was used.

## 2. Experimental

### 2.1. Materials

A commercial mesoporous silica (Davisil LC60A –Grace Davison, 60–200 μm) was used as a support of copper nanoparticles. A series of materials, denoted as Cu/SiO<sub>2</sub>(N) (where N is the number of steps of copper deposition), with different copper loadings were obtained using the following procedure. The sample Cu/SiO<sub>2</sub>(1) was prepared by conventional incipient wetness impregnation of silica support with 0.4 M aqueous solution of Cu(NO<sub>3</sub>)<sub>2</sub>·6H<sub>2</sub>O (Sigma Aldrich) and further consecutive treatment in air at 620 K and in hydrogen at 773 K for 1 h in each procedure. The Cu/SiO<sub>2</sub>(2) sample was obtained from Cu/SiO<sub>2</sub>(1) by OMCVD of bis-(hexafluoroacetylacetone) copper (II) hydrate (Cu(hfac)<sub>2</sub>, Strem Chemicals) following a modified procedure, described in [84]. In particular, the catalyst Cu/SiO<sub>2</sub>(1) was placed in a round bottom flask with an open holder on the bottom where Cu(hfac)<sub>2</sub> precursor was loaded to avoid any direct contact with the catalyst before sublimation. The powder was gently mixed by a rotary evaporator at 403 K in H<sub>2</sub> (800 mbar) for 3 h placing the flask inside an oil bath. After deposition, the catalyst was slowly heated (1.5 K min<sup>-1</sup>) up to 623 K in H<sub>2</sub> for precursor decomposition. The Cu/SiO<sub>2</sub>(3), Cu/SiO<sub>2</sub>(4) and Cu/SiO<sub>2</sub>(5) samples were prepared repeating the deposition/decomposition steps procedure using as a starting material the one obtained in the (N – 1) step.

After each synthesis the carbon content was determined by chemical analysis to be sure that no contaminations due to partial ligand decomposition occur. The copper content and carbon contaminants for each material are summarized in Table 1. Residual fluorine content was checked by XPS analysis, spectra were acquired in an M-probe apparatus (Surface Science Instruments), and the source was a monochromatic Al K $\alpha$  radiation (1486.6 eV). The binding energy (BE) was corrected for specimen charging by referencing the C 1s peak to 284.6 eV.

**Table 1**

Copper loading and carbon contaminants for various samples.

| Sample                  | Cu (wt%) <sup>a</sup> | C (wt%) <sup>b</sup> | Mean particle size <sup>c</sup> (nm) |
|-------------------------|-----------------------|----------------------|--------------------------------------|
| Cu/SiO <sub>2</sub> (1) | 1.4                   | 0.20                 | 2.04                                 |
| Cu/SiO <sub>2</sub> (2) | 3.3                   | 0.14                 | 2.77                                 |
| Cu/SiO <sub>2</sub> (3) | 4.9                   | 0.27                 | 3.29                                 |
| Cu/SiO <sub>2</sub> (4) | 5.7                   | 0.23                 | 3.42                                 |
| Cu/SiO <sub>2</sub> (5) | 6.7                   | 0.20                 | 3.62                                 |

<sup>a</sup> Determined by AAS.<sup>b</sup> From elemental analysis.<sup>c</sup> From TEM analyses.

## 2.2. Methods of investigation

Copper content in the samples was determined by Atomic Absorption Spectroscopy (AAS) with a Perkin Elmer-3100 Spectrometer using air-acetylene flame. Specific surface area and pore size distribution were measured through Nitrogen adsorption-desorption isotherms at 77 K using Micromeritics ASAP 2000 Analyser. Surface areas were calculated on the basis of the BET equation, whereas the pore size distribution was determined by the BJH method applied to the adsorption branch of the isotherm. Prior to the analysis, the samples were outgassed overnight at 573 K. The UV-Vis spectra of the powder samples were recorded using a Jasco V-650 spectrophotometer equipped with a diffuse reflectance unit. The temperature-programmed reduction-thermogravimetric (TPR-TG) analyses were performed with a Setaram TG 92 instrument. Before the experiments, the samples were reoxidized in air at 623 K for 1 h. Typically, 40 mg of the reoxidized sample were placed in a microbalance crucible and heated in a flow of 100 cm<sup>3</sup> min<sup>-1</sup> H<sub>2</sub> in Ar (1:1) up to 873 K at 5 K min<sup>-1</sup> and a final hold-up of 1 h. The weight loss during the reduction was calculated on the base of TPR-TG curves and the values were normalized to the same catalyst weight (40 mg). Temperature Programmed Reduction Decomposition – Mass Spectrometry analyses (TPRD-MS) were performed in a home made apparatus equipped with a quadrupole MS detector (HPR-20 QIC gas analysis mass spectrometer system/Hiden Analytical Ltd.) loading 70 mg of the sample in a U-shape pyrex reactor, connected upstream to a gas feeding device [85] under 5 vol% H<sub>2</sub> in He (30 cm<sup>3</sup> min<sup>-1</sup>) flow at a heating rate of 1.5 K min<sup>-1</sup>.

TEM micrographs were collected by a ZEISS LIBRA 200 FE HRTEM. Samples were gently grounded in an agate mortar and dispersed in isopropyl alcohol for 15 min in ultrasonic bath. A drop of each fine suspension was then deposited on a holey carbon film supported on a standard copper grid. TEM analyses were performed after complete evaporation of the solvent overnight. The frequency counts of metal NPs with respect to the diameter and mass percentage (simple spherical model [86]) were evaluated from several pictures representative of the catalyst.

FTIR spectra were recorded with a Nicolet Avatar 360 spectrometer accumulating 128 scans at a spectral resolution of 2 cm<sup>-1</sup>. Self-supporting pellets (ca. 10 mg cm<sup>-2</sup>) were prepared from the powdered sample and treated *in situ* in a purpose-made IR cell allowing measurements at ambient and low temperatures. The cell was connected to a vacuum-adsorption apparatus with a residual pressure below 10<sup>-3</sup> Pa. Prior to the adsorption experiments, the samples were evacuated at 673 K for 1 h. CO adsorption was performed at 100 K or at ambient temperature. In situ methanol decomposition experiments were performed with methanol (1 kPa equilibrium pressure) introduced to the catalyst at room temperature. Then the system was heated to 573 K for 10 min in methanol atmosphere and cooled to ambient temperature.

## 2.3. Catalytic experiments

Methanol conversion was carried out in a fixed bed flow reactor (0.055 g of catalyst), argon was used as a carrier gas (50 cm<sup>3</sup> min<sup>-1</sup>).

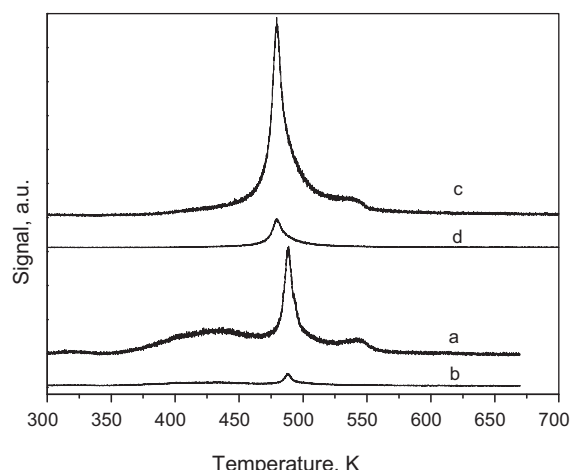


**Fig. 1.** TPRD pattern after the deposition of Cu(hfac)<sub>2</sub> on SiO<sub>2</sub> (a:  $m/z=69$ ; b:  $m/z=139$ ) and Cu/SiO<sub>2</sub> (c:  $m/z=69$ ; d:  $m/z=139$ ).

The methanol partial pressure was 1.57 kPa. The catalysts were tested under conditions of a temperature-programmed regime within the range of 350–770 K with heating rate of 1 K min<sup>-1</sup>. On-line gas chromatographic analyses were performed on HP apparatus equipped with flame ionization and thermo-conductivity detectors, on a PLOT Q column, using an absolute calibration method and a carbon based material balance. The product selectivities were calculated as  $X_i/X^*100$ , where  $X_i$  was the current yield of the product i and X was methanol conversion. The specific activity of the catalysts (SA) was calculated as the number of converted methanol molecules per a copper atom (%).

## 3. Results

### 3.1. TPRD-MS experiments

The mechanism of interaction of the Cu(hfac)<sub>2</sub> precursor with different samples was followed by TPRD-MS technique. The TPRD-MS data after the OMCVD deposition of Cu(hfac)<sub>2</sub> precursor on the parent silica support (a and b) and Cu/SiO<sub>2</sub>(1) (c and d) are presented in Fig. 1. The gaseous evolution pattern of fragments  $m/z=69$  (CF<sub>3</sub>) (Fig. 1a and c) and  $m/z=139$  (hfach-69) (Fig. 1b and d)), which are characteristic of precursor decomposition, were registered [87]. The fragments  $m/z=119$  (hfach-CF<sub>3</sub>-HF), 28 (CO), 44 (CO<sub>2</sub>), 16 (CH<sub>4</sub>), 12 (C), 15 (CH<sub>3</sub>) and 31(CF) were also detected (not shown). Both on SiO<sub>2</sub> and Cu/SiO<sub>2</sub>(1) the decomposition/desorption process mainly occurred in the range of 330–573 K. No desorption of Cu containing species was revealed by monitoring the fragments  $m/z=63$  and  $m/z=65$ , characteristic of atomic copper (not shown). On pure silica support the decomposition of Cu(hfac)<sub>2</sub> precursor was a step-wise process. The profile of  $m/z=69$  and 139 fragments (Fig. 1a and b) represented a broad peak in the range of 340–473 K, followed by a sharp one above 473 K. A small peak was also detected at higher temperature for  $m/z=69$  and for  $m/z=28$ , 44, 16, 12, 15 and 31 (not shown). The TPRD profile of Cu(hfac)<sub>2</sub> precursor, deposited on Cu/SiO<sub>2</sub>(1), consisted of a sharp peak at 463 K for fragments  $m/z=69$  and 139 (Fig. 1b and d) and a high temperature peak for  $m/z=69$ , 28, 44, 16, 12, 15 and 31, similar to pure silica. Note, that contrary to pure silica support, for the Cu/SiO<sub>2</sub>(1) sample, a low temperature effect in the range 340–473 K was not registered, which indicates differences in the deposition mechanism for both materials. Based on the above results and in order to minimize the carbonaceous residues during the synthesis and to obtain product with small amount of contaminants, a reduction temperature of 623 K was chosen for precursor decomposition (Table 1).

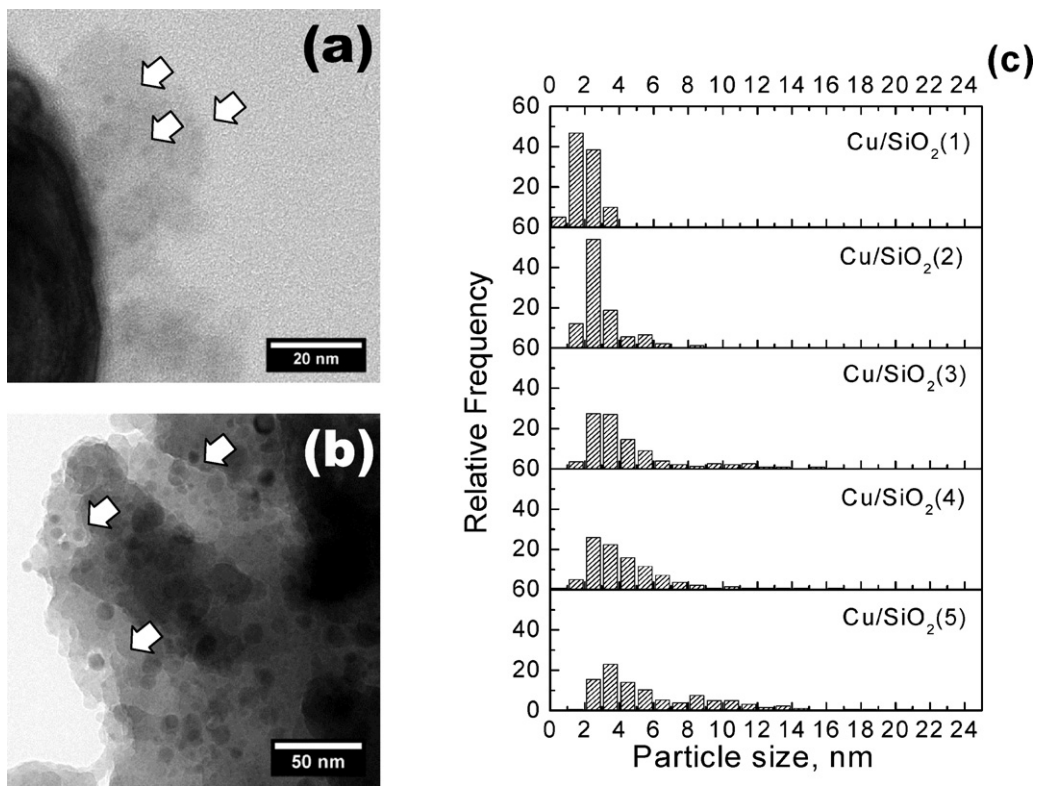


**Fig. 2.** TEM images of Cu/SiO<sub>2</sub>(1) (a) and Cu/SiO<sub>2</sub>(5) (b) and histograms of particles size distribution (calculated as relative mass-weighted frequency) in 0–25 nm region (c).

### 3.2. Structural characterization

#### 3.2.1. TEM

Among the various methods for characterization of materials in nanoscale, TEM has become a routine methodology, coupling direct observation of the particles with determination of their size distribution [88]. Some representative TEM images of copper-containing samples at lowest and highest metal loadings are shown in Fig. 2a and b, respectively. The copper NPs appeared as dark spots with predominantly spherical shape, which are uniformly distributed on the support. The materials showed a good stability under the electron beam during the measurements. The copper particle size distribution, calculated as relative mass-weighted frequency, is presented in Fig. 2c. The mean particle diameter increased and the distribution became broader with the increase of the copper content. At the lowest copper loading (sample Cu/SiO<sub>2</sub>(1)), the copper particles exhibited a narrow size distribution in the range of 0.9 to 3.8 nm, the majority of the particles being between 1 and 3 nm. With the Cu/SiO<sub>2</sub>(2) sample the minimum particle size increases to 1.3 nm and the fraction below 2 nm significantly decreased. At the same time particles close and above the pore diameter (up to 9 nm) appeared. Further increase of the minimum particle size (to 1.7 nm) was observed with the Cu/SiO<sub>2</sub>(3) sample and more large particles, evidently located onto the outer silica surface, were detected. Surprisingly, with the Cu/SiO<sub>2</sub>(4) sample again some particles just below 1 nm (minimal size of 0.98 nm) appeared again and the relative concentration of particles between 1 and 2 nm increased. Only few particles below 2 nm were detected with the Cu/SiO<sub>2</sub>(5) sample and, in this case, the relative concentration of bigger particles was important.

#### 3.2.2. Nitrogen physisorption

In order to obtain more information on the location of copper NPs into the support host matrix, a nitrogen physisorption study was carried out (Table 2 and Fig. S1, supplementary data). The

adsorption-desorption isotherms of the parent silica material was of type IV with a well pronounced step between 0.6 and 0.8 relative pressure and H<sub>2</sub> hysteresis loop, which is typical of mesoporous materials with ink-bottle-like pores. After the copper deposition, the curves did not change significantly in their shape, indicating a preservation of the support structure. However, even for the sample with the lowest copper loading, Cu/SiO<sub>2</sub>(1), the BET surface was decreased by ca. 20% and the pore volume, by ca. 10% (Table 2). We relate this observation to the location of copper particles predominantly inside the porous structure. This assumption correlates well with the data for the diameter of the particles, estimated by TEM measurements, which was much below the average pore diameter of the support (Tables 1 and 2). A simultaneous decrease in the pore volume (20%) and BET surface area (24%) was registered after the first OMVCD step (sample Cu/SiO<sub>2</sub>(2)). This indicates, in agreement with the TEM data (see above), a pore blocking due to particles growing up to size about the pore diameter. Further pore blocking and location of copper NPs on the outer surface could be assumed for Cu/SiO<sub>2</sub>(4) taking into account the strong decrease of the pore size (38%) and the surface area (40%) as compared with the pure silica (Fig. 2, Table 2). The effect of next step of OMVCD loading (sample Cu/SiO<sub>2</sub>(5)) is lower, pore size decrease is 35%, while the surface area decrease is 38% (Table 2). In agreement with

**Table 2**

BET surface area, pore volume and average pore diameter of the initial silica support and different copper modifications.

| Sample                  | BET surface area<br>(m <sup>2</sup> /g) | Pore volume<br>(cm <sup>3</sup> /g) | Average pore<br>diameter (nm) |
|-------------------------|-----------------------------------------|-------------------------------------|-------------------------------|
| SiO <sub>2</sub>        | 518                                     | 0.75                                | 5.6                           |
| Cu/SiO <sub>2</sub> (1) | 408                                     | 0.68                                | 5.8                           |
| Cu/SiO <sub>2</sub> (2) | 394                                     | 0.60                                | 5.6                           |
| Cu/SiO <sub>2</sub> (4) | 308                                     | 0.54                                | 6.2                           |
| Cu/SiO <sub>2</sub> (5) | 323                                     | 0.56                                | 5.9                           |

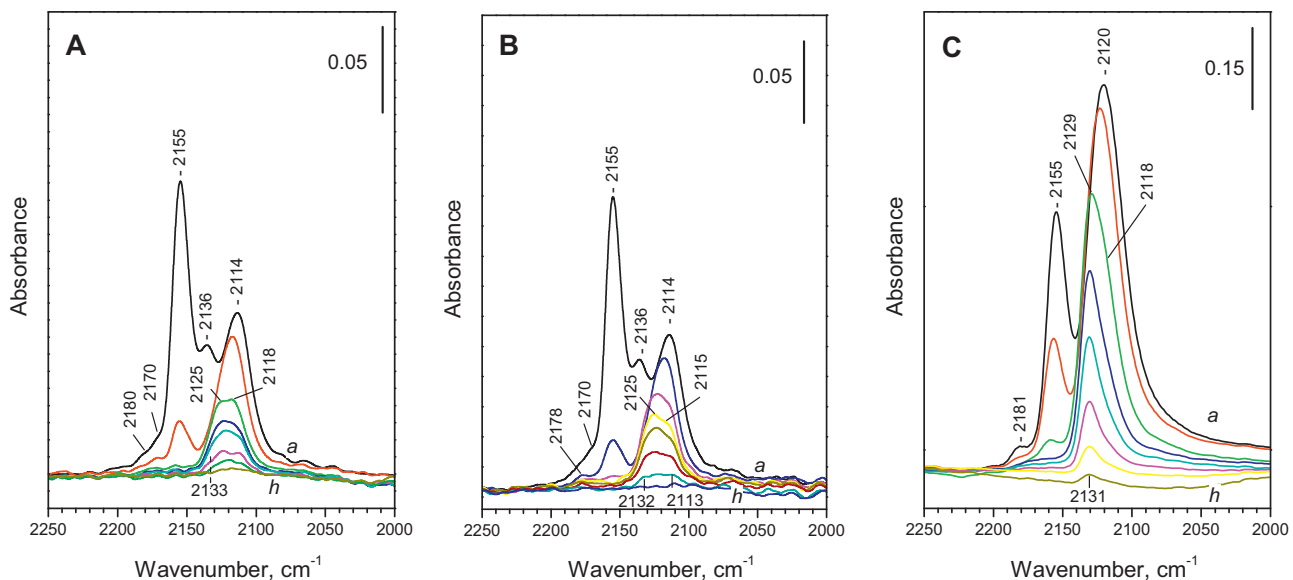


**Fig. 3.** IR spectra of CO adsorbed at 100 K on samples evacuated at 673 K: Cu/SiO<sub>2</sub>(1) (A), Cu/SiO<sub>2</sub>(2) (B) and Cu/SiO<sub>2</sub>(4) (C). Equilibrium pressure of 150 Pa (a) and evolution of the spectra under dynamic vacuum and increasing temperature up to RT (b–h).

the TEM data, this could be due to the growing of copper particles predominantly on the outer surface.

### 3.3. Spectroscopic data

#### 3.3.1. UV-Vis

The diffuse reflectance UV-Vis spectra of all materials studied (Fig.S2, supplementary data) contained an absorption peak at about 520 nm, which is generally assigned to plasmon resonance in copper nanoparticles with specific electronic properties [89]. Weak absorption bands in the 240–450 and 600–800 nm region (due to Cu<sup>2+</sup> → O<sup>2-</sup> charge-transfer transitions and d-d transitions, respectively, of copper oxide) could suggest existence of some Cu<sup>2+</sup> species [90–92].

#### 3.3.2. FTIR spectra of adsorbed CO

Adsorption of CO on the samples Cu/SiO<sub>2</sub>(1) and Cu/SiO<sub>2</sub>(2) at 100 K led to the appearance of a series of bands, at 2180, 2170, 2155, 2136 and 2114 cm<sup>-1</sup> (Fig. 3A and B). The bands at 2155 and 2136 cm<sup>-1</sup> easily disappeared during evacuation and were assigned to CO attached to silanol groups and physically adsorbed CO, respectively [93]. Indeed, these bands were observed after CO adsorption on the pure support. The low intensity bands at 2180–78 and 2170 cm<sup>-1</sup> (not detected with the support) were also unstable and could be assigned to Cu<sup>2+</sup>-CO carbonyls [93–95]. They were also observed with samples reduced with H<sub>2</sub> at 573 K (Fig. S3, supplementary data). Thus, these bands could be associated with finely dispersed Cu<sup>2+</sup> species strongly interacting with the silica support and thus being highly resistant to reduction. The band at 2114 cm<sup>-1</sup> was the most stable one and disappeared upon evacuation at higher temperatures (close to ambient one). According to the literature data [96] it is characteristic of Cu<sup>0</sup>-CO complexes. With coverage decrease the band was slightly blue shifted and finally splits into three bands, at ca. 2130, 2125 and 2115 cm<sup>-1</sup> (Fig. 3A and B). Similar triplet was also observed after adsorption of CO at ambient temperature (Fig. S4, supplementary data), but at somewhat lower wavenumbers (at 2125, 2120 and 2113 cm<sup>-1</sup>). The stability of the bands slightly decreased with the wavenumber increase. This could be explained with the fact that the π-component predominates in the Cu<sup>0</sup>-CO bond. The bands could be attributed to CO adsorbed on different Cu<sup>0</sup> sites on the metal particles (e.g. defect, step sites,

etc.) or can be associated with different sized particles [96]. In fact, Cu<sup>+</sup>-CO species could be detected in the same region, but the preservation of the spectra with the hydrogen-reduced sample supported the assignment of the bands under consideration to Cu<sup>0</sup>-CO carbonyls. Note, that the bands of copper carbonyls observed with both Cu/SiO<sub>2</sub>(1) and Cu/SiO<sub>2</sub>(2) samples were of similar intensities (Fig. 3A and B) despite the different copper loading (Table 1). This observation indicated that part of the copper sites in the Cu/SiO<sub>2</sub>(2) sample were not accessible to CO and suggested that copper was partly blocked in the silica pores. This was consistent with the assumption based on the TEM results and the Nitrogen physisorption data (Fig. S1, Table 2).

The IR spectrum of CO adsorbed at low temperatures on the Cu/SiO<sub>2</sub>(4) sample (prepared by three repeated OMCVD procedures) contained three bands at 2182, 2155 and 2120 cm<sup>-1</sup> (Fig. 3C). The band at 2182 cm<sup>-1</sup> easily disappears during evacuation and can be attributed to Cu<sup>2+</sup>-CO species. This band was not observed with the sample reduced with H<sub>2</sub> at 673 K which was consistent with the TPR results. Most probably the Cu<sup>2+</sup> sites have been formed as a result of a partial reoxidation of copper during exposure of the sample to air. In addition, the band at 2182 cm<sup>-1</sup> was observed here with much higher intensity as compared with the Cu/SiO<sub>2</sub>(1) and Cu/SiO<sub>2</sub>(2) samples (Fig. 3), i.e. in this case a high amount of oxidized copper existed. The band at 2120 cm<sup>-1</sup> (sample Cu/SiO<sub>2</sub>(4)) was shifted to higher frequencies (ca. 2131 cm<sup>-1</sup> at very low coverage) and a shoulder at ca 2118 cm<sup>-1</sup> became visible with coverage decrease. In contrast to the Cu/SiO<sub>2</sub>(1) and Cu/SiO<sub>2</sub>(2) samples, the high frequency (HF) component at ca. 2130 cm<sup>-1</sup> was more stable than the low frequency (LF) one. Also, the band around 2120 cm<sup>-1</sup> was definitely more intense as compared to the 2114 cm<sup>-1</sup> band observed with the Cu/SiO<sub>2</sub>(1) and Cu/SiO<sub>2</sub>(2) samples, more than expected on the basis on the increased copper content. This suggested contribution of Cu<sup>+</sup>-CO species to the envelope at 2130 cm<sup>-1</sup> [93]. The supposition was also supported by the fact that the component at 2130 cm<sup>-1</sup> was more stable than the Cu<sup>0</sup>-CO bands observed with the other two samples. A careful analysis of the spectra revealed that, after short evacuation at 100 K, weak bands at 2175 and 2162 cm<sup>-1</sup> were distinguished. They could be associated with the symmetric CO modes of Cu<sup>+</sup>(CO)<sub>2</sub> dicarbonyl species [93], the corresponding asymmetric mode being in the range of monocarbonyls. These two bands (shifted to 2158 and 2170 cm<sup>-1</sup>)

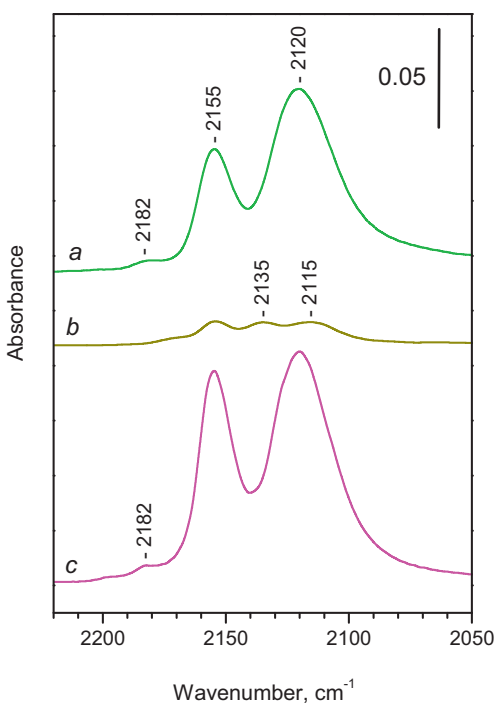


**Fig. 4.** IR spectra of CO adsorbed (150 Pa) at 100 K on sample Cu/SiO<sub>2</sub>(4): evacuated at 673 K (a), undergone interaction with methanol at 573 K (b) and reoxidized in air at 673 K (c).

were better seen in the spectra of CO adsorbed at ambient temperature (Fig. S4, supplementary data). The above results indicated that the copper particles in Cu/SiO<sub>2</sub>(4) were reoxidized to Cu<sup>2+</sup> and Cu<sup>+</sup> species.

In order to check the state of the copper after interaction of the samples with methanol, we tested the surface with CO as a probe molecule. It was established that, after interaction of Cu/SiO<sub>2</sub>(4) sample with methanol at 573 K, copper was reduced and agglomerated: the Cu<sup>0</sup>–CO band at 2115 cm<sup>-1</sup> was detected with a very low intensity (Fig. 4). Also, the band at 2155 cm<sup>-1</sup> (OH-CO species) appeared with strongly reduced intensity while the Si-OH band remained practically unaffected. This observation indicated that a large fraction of the silanol groups had become inaccessible, i.e. they were blocked in the pores by copper particles. Subsequent interaction with air at 673 K led to reoxidation and redispersion of copper and to a sharp increase of the accessibility of the silanol groups. These effects were hardly observed with the Cu/SiO<sub>2</sub>(2) sample showing different response of copper to the treatment.

### 3.4. TPR measurements

#### 3.4.1. TPR study of the initial materials

It was well established that the reduction of bulk metal oxides is easier for the smaller particles [97–99]. Generally, for the supported materials, the picture is more complicated because the reduction process is affected by the interaction between the supported phase and the support. As a rule, isolated cations are more difficultly reduced than associated ones.

Our preparation technique presupposes obtaining of the samples in reduced state. That is why, before the TPR experiments, all the samples were subjected to a standard pre-treatment consisting of oxidation in air at 623 K for 1 h. The TPR-TG and TPR-DTG profiles of all materials are presented in Fig. 5 a and c and the corresponding TPR data are listed in Table 3. The main reduction effects for all materials were observed in the range 400–600 K which, according to [92,97] were assigned to one-step Cu<sup>2+</sup> → Cu<sup>0</sup>

**Table 3**  
TPR-TG data for different modifications.

| Sample                  | T <sub>max</sub> (K) | Weight loss (mg) | Reduction degree (wt%) |
|-------------------------|----------------------|------------------|------------------------|
| Cu/SiO <sub>2</sub> (1) | 486                  | 0.09             | 64                     |
| Cu/SiO <sub>2</sub> (2) | 464, 503             | 0.30             | 91                     |
| Cu/SiO <sub>2</sub> (3) | 469                  | 0.50             | 100                    |
| Cu/SiO <sub>2</sub> (4) | 454                  | 0.67             | 100                    |
| Cu/SiO <sub>2</sub> (5) | 455                  | 0.79             | 100                    |

transition. For the sample Cu/SiO<sub>2</sub>(1) the weight loss corresponded to 64% reduction of loaded copper and the TPR-DTG peak maximum was detected at 486 K (Table 3). The low reduction degree could be due to two reasons: (i) not complete reoxidation of copper at the standard conditions applied and/or (ii) presence of a hardly reducible Cu<sup>2+</sup> species in strong interaction with the silica support. In order to discriminate between the two possibilities we have studied a Cu/SiO<sub>2</sub>(1) sample preoxidized at 773 K. The results (Fig. S5, supplementary data) showed that in this case the copper reduction degree was even lower. Therefore, we conclude that hardly reducible Cu<sup>2+</sup> species, probably isolated cations, existed on the sample and this was in agreement with the FTIR data (Fig. 3). Although some of these species could have been produced during the sample preparation procedure, it is evident that part of them are formed as a result of reoxidation of some finely dispersed metal copper particles.

About 90% degree of reduction and two well distinguished DTG effects, one of them shifted to lower and the other to higher temperatures, as compared to the Cu/SiO<sub>2</sub>(1) sample, were registered for Cu/SiO<sub>2</sub>(2) (Fig. 5c). These features could be related to the reduction of copper oxide-like particles with different dispersion. In agreement with literature data [97–99], the low-temperature peak could be due to the reduction of larger, and the second one, to the reduction of smaller oxide particles. The existence of smaller particles can be rationalized assuming formation of oligomers with the participation of the isolated copper ions (that have existed in Cu/SiO<sub>2</sub>(1) sample before the second copper loading reduction). This accounted for the increasing the copper reduction degree.

The increase in the number of the OMCVD steps for the Cu/SiO<sub>2</sub>(3) and Cu/SiO<sub>2</sub>(4) materials led to progressive shifting of the DTG profile to lower temperatures with a 100% reduction degree (Fig. 5c, Table 3), which indicated additional increase in the copper oxide particle size. The main DTG peaks were observed practically at the same temperature for the Cu/SiO<sub>2</sub>(4) and Cu/SiO<sub>2</sub>(5) samples, which indicated appearance of larger bulk-like copper oxide particles. However, the decrease of the TG profile of the Cu/SiO<sub>2</sub>(4) above 650 K (Fig. 5a) suggested that some atomically dispersed species were present in this sample.

#### 3.4.2. TPR study of materials used in catalytic reaction. Redox changes with the samples

The TPR data of the materials used in the catalytic test after standard oxidation treatment are presented in Fig. 5b and d. The samples Cu/SiO<sub>2</sub>(2) and Cu/SiO<sub>2</sub>(3) exhibited 100% reduction in the 400–600 K temperature interval and the TPR-DTG effects became narrow and slightly shifted to lower temperatures as compared to those of the parent materials. This indicated that the copper oxide particles became larger and more uniformly dispersed, evidently as a result of the exposure of the catalyst to the reaction medium.

With the Cu/SiO<sub>2</sub>(1) sample (Fig. 5c) the main TG effect occurred at 613 K, at temperature significantly higher as compared to the initial sample (Fig. 5a). At the same time, the degree of reduction increased to 85%. This observation could be explained by redispersion of the larger metal particles and, at the same time, agglomeration of isolated ions (left on the sample after preparation) during catalytic test. Similar fraction of hardly reducible species

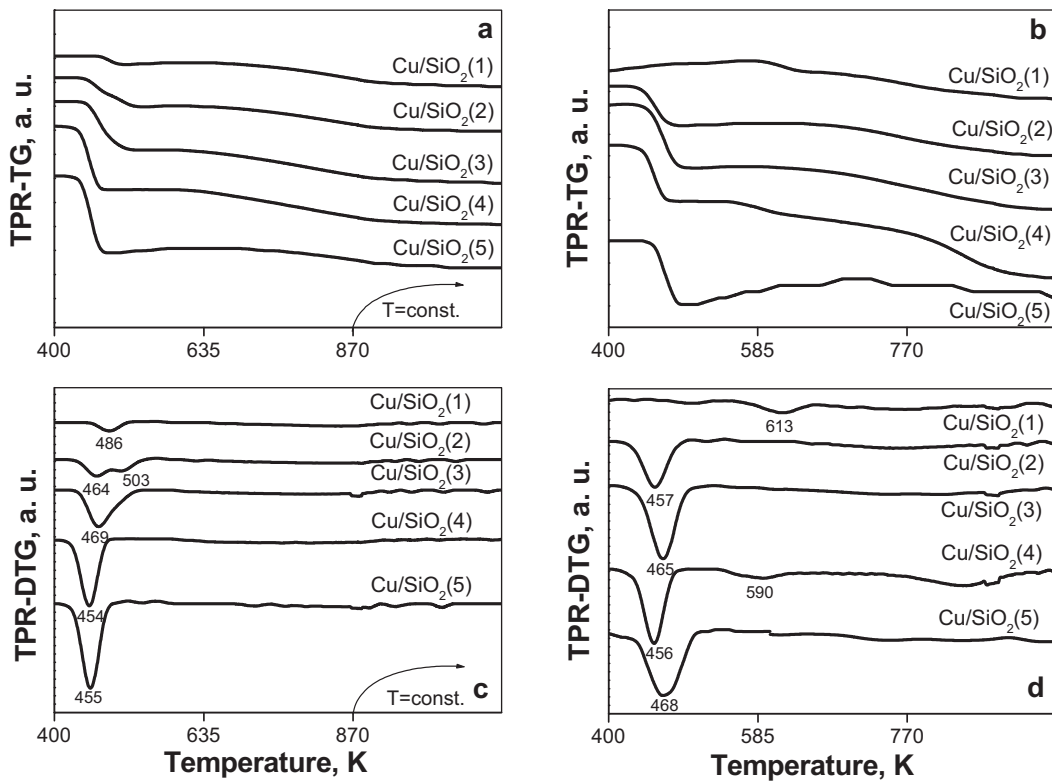


**Fig. 5.** TPR-TG and TPR-DTG profiles of reoxidized initial (a and c) and used in catalysts (b and d) copper modifications, respectively.

was detected for Cu/SiO<sub>2</sub>(4). In this case, due to the high copper concentration, no isolated cations were detected.

The TPR-DTG profile of the sample with the highest copper loading, Cu/SiO<sub>2</sub>(5) (Fig. 5d), was, contrary to the profiles of the other samples, significantly broadened, indicating formation of non uniformly dispersed particles due to intense migration of copper species on the outer surface. Therefore, we can conclude that the uniform distribution with the samples Cu/SiO<sub>2</sub>(2) and Cu/SiO<sub>2</sub>(3) is probably assisted by the support porous structure.

### 3.5. Catalytic experiments

#### 3.5.1. Methanol decomposition in a flow fixed bed reactor

Data on methanol decomposition for various materials, which were registered under temperature programmed regime (1 K min<sup>-1</sup>) in a range 400–750 K are presented in Fig. 6. The main carbon containing product from the decomposition was CO (Fig. 6b), but methane and CO<sub>2</sub> were also registered as byproducts.

The position of the conversion curves (Fig. 6a) indicated the best catalytic activity and selectivity to CO for Cu/SiO<sub>2</sub>(4) in the whole investigated interval, while the catalytic activity and selectivity were the lowest for Cu/SiO<sub>2</sub>(2). We should stress on the steep shape of the conversion curve for the Cu/SiO<sub>2</sub>(1) sample above 700 K, where similarly to the sample Cu/SiO<sub>2</sub>(4), about 90% conversion was achieved, despite the large difference (more than 3 times) in the copper loading (Fig. 6a). In order to precise the catalytic data, the specific activity was calculated per a copper atom for selected temperatures (Fig. 7). Two general effects should be pointed out:

- (i) the sample Cu/SiO<sub>2</sub>(1) demonstrated the highest specific catalytic activity in the whole temperature interval, followed by the Cu/SiO<sub>2</sub>(4) sample;
- (ii) the specific activity of Cu/SiO<sub>2</sub>(1) enormously increased above 700 K, while the temperature effect on the specific activity for the other materials was significantly lower.

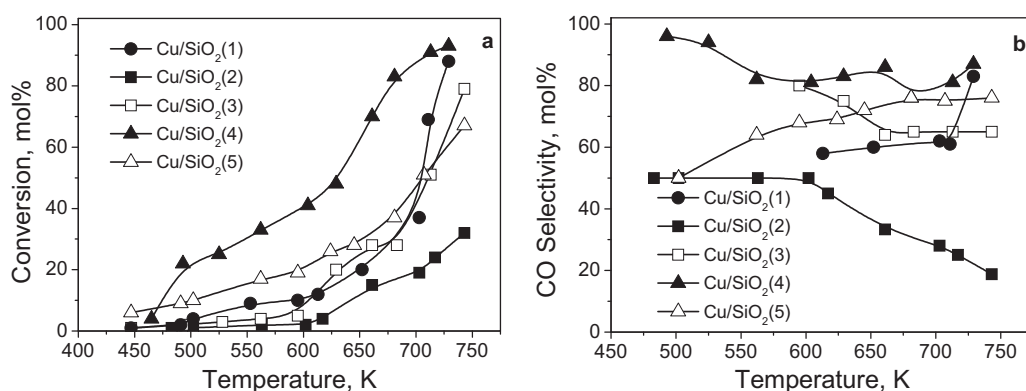


**Fig. 6.** Methanol conversion (a) and CO selectivity (b) vs. temperature for the studied samples.

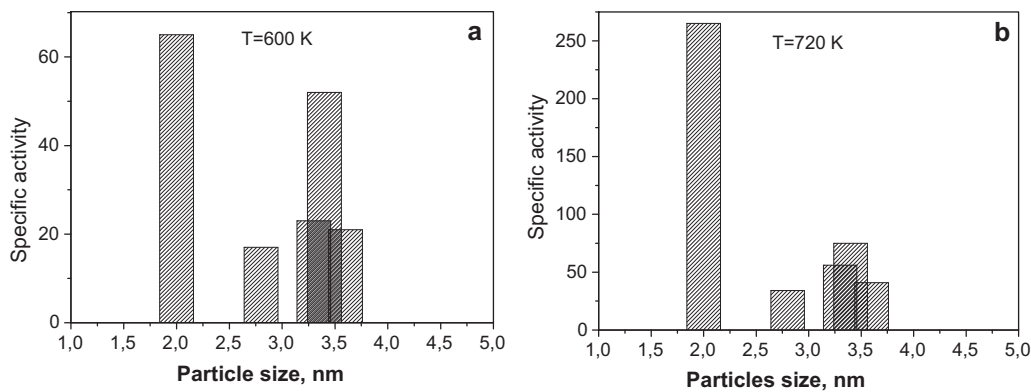


Fig. 7. Specific activity dependence of copper particles size at 600 K (a) and 720 K (b).

### 3.5.2. In situ FTIR methanol decomposition investigation in static conditions

FTIR in situ measurements of methanol decomposition for selected materials were performed after introduction of methanol (10 mbar equilibrium pressure) at RT to the catalyst followed by heating to 573 K for 10 min. The gas phase spectrum analysis (Fig.S6, supplementary data) showed formation of CO ( $2143\text{ cm}^{-1}$ ) and H<sub>2</sub>CO (3470, 2820, 2750 and  $1745\text{ cm}^{-1}$ ) over all catalysts. The intensity of product bands registered after methanol decomposition for 10 min at 573 K increased in the sequence: Cu/SiO<sub>2</sub>(2) < Cu/SiO<sub>2</sub>(4) < Cu/SiO<sub>2</sub>(1), which correlated well with the arrangement of the samples according to their specific activity during the conventional catalytic test (see above).

After the experiment with methanol decomposition the Cu/SiO<sub>2</sub>(4) sample was successively treated at 673 K in (i) air and (ii) H<sub>2</sub> and then evacuated at the same temperature. H<sub>2</sub>-reduced sample demonstrated much higher activity than activated one. This suggested that oxidized Cu<sup>2+</sup> containing species are less active in this reaction and activation of the Cu/SiO<sub>2</sub> catalyst towards methanol decomposition require reduction of the copper.

## 4. Discussion

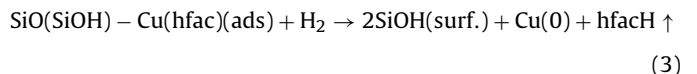
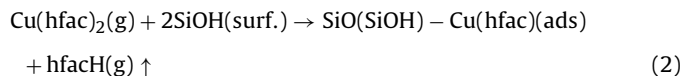
The majority of the studies on OMCVD for the preparation of supported catalysts concern the employment of a fluidized bed reactor [74,75] even if few examples of rotary bed reactor were reported too [84]. The main problems encountered with flowing technique are related to the poor control in the metal loading due to a relevant decomposition of the precursor on the inner walls of the reactor as well as to the complexity of the design and realization of the apparatus for this procedure. In this study, we adopted small scale synthetic methodology for the tailored preparation of copper NPs supported on mesoporous silica using only commercial laboratory equipment. Copper precursor (Cu(hfac)<sub>2</sub>) is a commercially available substance, which is largely utilized for the deposition of Cu films. The application of Cu(hfac)<sub>2</sub> precursor required the presence of hydrogen to assure the deposition of copper in metallic state, according to the simplified reaction (1) [100–102]:



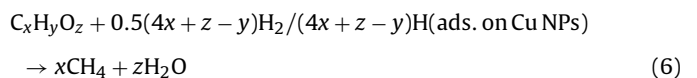
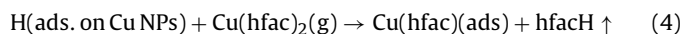
It is well known that metallic surfaces promote the above mechanism [103,104]. We performed the OMCVD under static H<sub>2</sub> atmosphere at low temperature to avoid the complete decomposition of the precursor during its interaction with the solid sample. This strategy allowed the precursor to interact with the surface sites of the metallic Cu NPs in an optimal way thus giving rise to well dispersed, probably isolated species. In order to control the dimension of copper NPs on silica, we carried out a multi-step deposition process of Cu(hfac)<sub>2</sub> starting from a parent copper loaded

material, simply obtained by wetness impregnation technique. The TPRD analyses of Cu(hfac)<sub>2</sub> interaction with pure silica support and copper modified one (Fig. 1) clearly indicated that on the two materials the OMCVD process proceeded according to different mechanisms.

The broad peak in the range 340–473 K, which was only registered for the pure silica support, was due to Cu(hfac)<sub>2</sub> dissociation to Cu(hfac) and hfac ligand and further ligand desorption via protonation by the surface Si-OH groups according to reaction (2) [105–107]. A role of copper NPs can be excluded since, under the conditions here employed for the OMCVD process, the formation of metallic Cu is not likely to happen, as already reported by Hanaoka for deposition on SiO<sub>2</sub> at 473 K under pure H<sub>2</sub> [105]. The complete decomposition of adsorbed precursor, leading to Cu NPs, only occurs during the reduction treatment, at higher temperatures, according to reaction (3).



The Cu(hfac)<sub>2</sub> adsorption on support, and further decomposition to Cu NPs follows a different mechanism when OMCVD was performed on Cu/SiO<sub>2</sub> material. The absence of the first low temperature broad peak and the different shape of the TPRD profile for the copper modified silica (Fig. 1) clearly indicated that Cu(hfac)<sub>2</sub> precursor selectively interacted with the metal particles, where according to [105,108], the dissociative adsorption to Cu(hfac) and hfac, with further removal of one of the ligand assisted by activated hydrogen on the metal surface, occurred (react. (4)) already during OMCVD deposition at 403 K.



The complete decomposition of adsorbed Cu(hfac) fragment proceeds at high temperature, actually shifted with 10 K to lower temperature with respect to the one in bare silica, and can be attributed to a hydrogen promoted process also involving the metallic surface (react. (5)). Finally, the fragments detected above 523 K are associated to a reduction or decomposition of species adsorbed on the catalysts surface, as schematized in reaction (6).

On the basis of TPRD results the reductive decomposition treatment, leading to supported Cu NPs, was carried out at temperatures higher than 573 K in order to have a low level of carbon contaminants in the product (Table 1). Also fluorine incorporation in the support, as reported to occur using F-containing Cu precursors (like Cu(hfac)<sub>2</sub> here employed) [109], was not revealed, according to XPS measurements performed on the high loaded sample.

TEM measurements demonstrated that during the wetness impregnation of the porous silica support finely dispersed (up to 4 nm) copper nanoparticles were formed (sample Cu/SiO<sub>2</sub>(1)). Nitrogen physisorption and FTIR of adsorbed CO indicated that these NPs were stabilized mainly within the pores of the silica matrix. The chemical analyses (Table 1) of the samples confirmed that the applied step-wise strategy of OMCVD of Cu(hfac)<sub>2</sub> over this starting copper containing material allowed an increase in the amount of metal deposited through preferential interaction of Cu(hfac)<sub>2</sub> with the copper particles [105,110]. Materials with relatively uniform and size controlled metal copper nanoparticles were obtained with increasing of copper loading up to 6.7 wt% (Fig. 2 Table 1). The particles were mainly deposited into the mesopores of the support even when copper content increased up to 3.3 wt% (sample Cu/SiO<sub>2</sub>(2)). The increase in the copper content above 4 wt% led to deposition of copper particles with various dispersion on the outer silica surface (samples Cu/SiO<sub>2</sub>(3) and Cu/SiO<sub>2</sub>(4)), which readily grew after further increase in the copper loading (sample Cu/SiO<sub>2</sub>(5)). In addition to the large particles, which diameter went beyond that of the pores, it was evident that smaller particles were also formed on the outer surface. This was unambiguously proven by the increase of the number of particles with size below 2 nm in Cu/SiO<sub>2</sub>(4) as compared to the sample Cu/SiO<sub>2</sub>(3) (Fig. 2, Table 1).

Our results showed that the redox behaviour of the deposited copper particles strongly depended both on their size and location in the silica host matrix. Let us initially consider metal particles in the silica pores (samples Cu/SiO<sub>2</sub>(1) and Cu/SiO<sub>2</sub>(2)). Evidently, in this case, the metal state was stabilized and copper resisted oxidation at ambient temperature (Fig. 3). However, after oxidation in air at 623 K, finely dispersed oxidized copper species were produced and they strongly interacted with the silica support. This made their subsequent reduction with hydrogen difficult (Fig. 5). Comparing the data from TEM and TPR analyses we assume that this oxidation behaviour is typical of metal particles with a mean diameter around or slightly above 1 nm. Similar oxidation of metal particles was reported with supported silver, where atomically dispersed Ag<sup>+</sup> cations were produced [111].

As mentioned above, with increase of copper loading, part of copper particles were located on the outer silica surface. It seems that the smallest particles on the outer surface (as was the case of sample Cu/SiO<sub>2</sub>(4)), contrary to the case of similar small particles in the pores (samples Cu/SiO<sub>2</sub>(1) and Cu/SiO<sub>2</sub>(2)), were partially oxidized under atmospheric conditions even at ambient temperature. This was well illustrated by the formation of Cu<sup>+</sup> and Cu<sup>2+</sup> species with the Cu/SiO<sub>2</sub>(4) sample after oxidation at RT as evidenced by FTIR-CO measurements (Fig. 3). Similar effect of formation of small CuO aggregates and a shell of amorphous oxide layer around the metal core after the samples expose to air was observed with titania-supported copper [70]. It was also assumed that the latter species dominated for the samples with higher copper loading.

The elucidation of the size effect in catalysis was difficult because of several additional effects. Here the influence of reaction medium with rather complex composition and the possibility of restricted mass transfer to the active species, located within the porous structure should be taken into consideration. In any case, our results indicated size dependent effects during the methanol decomposition experiments. The sample characterized by copper particles with diameter up to 4 nm, Cu/SiO<sub>2</sub>(1), exhibited the

highest specific activity and high selectivity towards CO (Fig. 6). Note that, unlike the other samples, the specific activity for Cu/SiO<sub>2</sub>(1) increased more than 3 times when the temperature increased from 600 to 720 K (Fig. 7). The TPR patterns of the sample used in catalysis showed a well pronounced shift of the TPR-DTG profile to higher temperatures and increase in the reduction degree, as compared to the fresh sample (Fig. 5b and d). These results indicate formation of relatively small copper nanoparticles during the catalytic test which, under reoxidation, were converted to small CuO clusters, relatively strongly interacting with the support. We would like to stress again on the complex composition of the reaction medium (H<sub>2</sub>,CO, H<sub>2</sub>O, etc.), which differs from the pure reductive conditions of the OMCVD procedure [23,20]. The above observation can be rationalized assuming that, under the reaction medium, transport of copper species occurs. At first, larger particles are redispersed. Secondly, as a result of copper migration, isolated cations form associated species which enhances their reducibility. As a result, larger particles are redispersed and isolated species agglomerated. It is also probable that the particles obtained are characterized by a specific morphology and surface defects, as suggested in [23,20]. Rostovshchikova et al. [20] reported that the dependence of specific catalytic activity on the particle surface density exhibited a pronounced maximum when copper atoms were arranged in densely packed ensembles. As reported in [112], the catalytic function of copper in methanol decomposition is markedly different from those of Group VIII metals. The authors suggested that over copper catalysts methanol decomposed through methyl formate as an intermediate, while over Group VIII metals, directly to CO and H<sub>2</sub>. The difference in the catalytic performance was ascribed to the difference in the structure of adsorbed HCHO intermediates (mono- $\eta^1$  (O) and bi-dentate- $\eta^2$  (C,O), respectively). Guerreiro et al. [88] assumed that methanol dehydrogenation to methyl formate intermediate was related to the activity of certain geometric array (ensemble) that was only achieved by critical copper diameter, making this reaction structure sensitive. Alternatively, some authors proposed a mechanism of methanol decomposition involving the formation of surface methoxy species via interaction of methanol with oxygen adsorbed on the copper surface. Dehydrogenation of the methoxy species with the formation of adsorbed HCHO [113] and its further interaction with surface oxygen leading to the formation of methylenbisoxo species or, by reaction with methoxide, to methyl formate was proposed. We also detected HCHO species in our FTIR experiments. So, the observed behaviour of Cu/SiO<sub>2</sub>(1) provoked us to assume the highest catalytic activity for copper nanoparticles that form, after oxidation, small CuO clusters characterized by TPR peaks around 600 K. Most probably, these are particles below 1 nm but bigger particles having specifically arranged surface ensembles could also contribute to this. In both cases it seems that the catalytic activity could significantly increase with the increase of the structure defects, when the particles change under the influence of the redox reaction medium. The sample Cu/SiO<sub>2</sub>(2) with higher copper content contains no particles with size below 1 nm (Fig. 2). This can explain its lower catalytic activity. In addition, the nitrogen physisorption, TEM and FTIR data strongly indicated a significant pore blocking effect in this case due to the formation of particles with dimension close to the pore diameter of the support, which probably restricted the mass transfer of reaction atmosphere to the active sites. However, the particles with size below 1 nm appeared in the Cu/SiO<sub>2</sub>(4) (Fig. 2). We assumed their higher accessibility due to the location on the outer surface (see above). Again, as in the case of Cu/SiO<sub>2</sub>(1), they could agglomerate during the reaction and form highly defective structures, predominantly on the outer surface. This assumption is also well supported with the appearance of TPR effect at about 600 K for Cu/SiO<sub>2</sub>(4) after being subjected to a catalytic test (Fig. 5). An additional evidence was TEM images of Cu/SiO<sub>2</sub>(4) after the

catalytic test, where the mean particles size increased from 3.42 to 4.54 nm (see S7 in supporting information). Further growing of the particles on the outer surface with the copper loading increase for the Cu/SiO<sub>2</sub>(5) sample (Fig. 2) explained the decrease in the amount of these structures (Fig. 5) and the decrease in the catalytic activity.

## 5. Conclusion

A novel method for the synthesis of high surface area porous silica supported copper nanoparticles with tailored size was developed. The method is based on the selective step-wise chemical vapor deposition and decomposition of Cu(hfac)<sub>2</sub> precursor, under hydrogen atmosphere, onto a parent system consisting of pre-formed finely dispersed copper particles loaded on the silica support. The simple apparatus, the cheap and commercially available mesoporous support and copper precursor, the high copper loadings easily obtainable, the low level of carbon contaminants and, last but not least, the controlled metal particles size, are the main advantages of the proposed method.

Size dependent effects of the redox and catalytic properties of the loaded copper particles are also demonstrated, even if strongly affected by the location and accessibility of the particles in the porous structure. It is found that copper NPs change in size and defectivity under the reaction medium and the most active particles are highly defect. This process is partially counterbalanced by the pore blocking at high Cu loadings.

## Acknowledgements

Financial support of Bulgarian Academy of Science and National Scientific Fund of Ministry of Education, Projects DTK 02/64 and DO 02-290, and bilateral project BAS-CNR is acknowledged. M.M. also acknowledge support from the Alexander von Humboldt Foundation. Prof. C.L. Bianchi is strongly acknowledged for her assistance in XPS measurements.

## Appendix A. Supplementary data

Supplementary data associated with this article can be found, in the online version, at <http://dx.doi.org/10.1016/j.apcatb.2012.07.022>.

## References

- [1] M. Che, C.O. Bennett, *Advances in Catalysis* 36 (1989) 55–171.
- [2] R. Narayanan, M.A. El-Sayed, *Journal of Physical Chemistry B* 109 (2005) 12663–12676.
- [3] Yon Ju-Nam, Jamie R. Lead, *Science of the Total Environment* 400 (2008) 396–414.
- [4] J.M. Mayne, K.A. Dahlberg, T.A. Westrich, A.R. Tadd, J.W. Schwank, *Applied Catalysis A-General* 400 (2011) 203–214.
- [5] M. Boudart, M.A. McDonald, *Journal of Physical Chemistry* 88 (1984) 2185–2195.
- [6] M. Ojeda, S. Rojas, M. Boutonnet, F.J.P. Alonso, F.J.G. Garcia, J.L.G. Fierro, *Applied Catalysis A-General* 274 (2004) 33–41.
- [7] G.A. Somorjai, J.Y. Park, *Catalysis Letters* 115 (2007) 87–98.
- [8] M. Kobune, S. Sato, R. Takahashi, *Journal of Molecular Catalysis A: Chemical* 279 (2008) 10–19.
- [9] M. Mavrikakis, A.A. Gokhale, J.A. Dumesic, *Journal of the American Chemical Society* 130 (2008) 1402–1414.
- [10] G.A. Somorjai, N. Materer, *Topics in Catalysis* 1 (1994) 215–231.
- [11] J.Z. Zhang, Y.-T. Tsai, K.L. Sangkaewwattana, J.G. Goodwin Jr., *Journal of Catalysis* 280 (2011) 89–95.
- [12] M. Guidotti, V. Dal Santo, A. Gallo, E. Gianotti, G. Peli, R. Psaro, L. Sordelli, *Catalysis Letters* 112 (2006) 89–95.
- [13] J.H. Sinfelt, *Science* 195 (1977) 641–646.
- [14] G.R. Bamwenda, S. Tsubota, T. Nakamura, M. Haruta, *Catalysis Letters* 44 (1997) 83–87.
- [15] G.L. Bezemer, J.H. Bitter, H.P.C.E. Kuipers, H. Oosterbeek, J.E. Holewijn, X. Xu, F. Kapteijn, A.J. van Dillen, K.P. de Jong, *Journal of the American Chemical Society* 128 (2006) 3956–3964.
- [16] A. Lutz, R. Bradshaw, L. Broomeberg, A. Rabinovich, *International Journal of Hydrogen Energy* 29 (2004) 809–816.
- [17] G. Jones, J.G. Jakobsen, S.S. Shim, J. Kleis, M.P. Andersson, J. Rossmeisl, F. Abild-Pederson, T. Bligaards, S. Helveg, B. Hinemann, J.R. Rostrup-Nielsen, I. Chorkendorff, J. Sehested, J.K. Nørskov, *Journal of Catalysis* 259 (2008) 147–160.
- [18] H.S. Bengaard, J.K. Nørskov, J. Sehested, B.S. Clausen, L.P. Nielsen, A.M. Molenbroek, J.R. Rostrup-Nielsen, *Journal of Catalysis* 209 (2002) 365–384.
- [19] D.A.J.M. Ligthart, R.A. van Santen, E.J.M. Hensen, *Journal of Catalysis* 280 (2011) 206–220.
- [20] T.N. Rostovshchikova, V.V. Smirnov, V.M. Kozhevnik, D.A. Yavsin, M.A. Zabelin, I.N. Yassievich, S.A. Gurevich, *Applied Catalysis A-General* 296 (2005) 70–79.
- [21] B.G. Gates, *Chemical Reviews* 95 (1995) 511–522.
- [22] B. Coq, F. Figueras, *Coordination Chemistry Reviews* 178–180 (1998) 1753–1783.
- [23] A. Yu. Stakheev, L.M. Kustov, *Applied Catalysis* 188 (1999) 3–35.
- [24] C.R. Henry, *Applied Surface Science* 164 (2000) 252–259.
- [25] F.A. Pederson, O. Lytken, J. Engbæk, G. Nielsen, I. Chorkendorff, J.K. Nørskov, *Surface Science* 590 (2005) 127–137.
- [26] J. Wei, E. Iglesia, *Journal of Catalysis* 224 (2004) 370–383.
- [27] M.P. Andersson, F. Abild-Pedersen, I.N. Remediakis, T. Bligaard, G. Jones, J. Engbæk, O. Lytken, S. Horsch, J.H. Nielsen, J. Sehested, J.R. Rostrup-Nielsen, J.K. Nørskov, I. Chorkendorff, *Journal of Catalysis* 255 (2008) 6–19.
- [28] R. van Hardeveld, F. Hartog, *Surface Science* 15 (1969) 189–230.
- [29] H.H. Kung, M.C. Kung, *Catalysis Today* 97 (2004) 219–224.
- [30] Y. Matsumura, K. Tanaka, N. Tode, T. Yazawa, M. Haruta, *Journal of Molecular Catalysis A: Chemical* 152 (2000) 157–165.
- [31] J.R. Croy, S. Mostafa, J. Liu, Y. Sohn, B.R. Cuenya, *Catalysis Letters* 118 (2007) 1–7.
- [32] G.A. Olah, *Catalysis Letters* 93 (2004) 1–2.
- [33] P. Mizsey, E. Newson, T.B. Truong, P. Hottinger, *Applied Catalysis A-General* 213 (2001) 233–237.
- [34] K.W. Park, D.S. Han, Y.E. Sung, *Journal of Power Sources* 163 (2006) 82–86.
- [35] M. Borasio, O.R. de la Fuente, G. Rupprechter, H.J. Freund, *Journal of Physical Chemistry B* 109 (2005) 17791–17794.
- [36] H. Borchert, B. Jurgens, T. Nowitzki, P. Behrend, Y. Borchert, V. Zielasek, S. Giorgio, C.R. Henry, M. Baumer, *Journal of Catalysis* 256 (2008) 24–36.
- [37] J.C. Brown, E. Gulari, *Catalysis Communications* 5 (2004) 431–436.
- [38] W.Q. Cao, G.W. Chen, S.L. Li, Q. Yuan, *Chemical Engineering Journal* 119 (2006) 93–98.
- [39] J.R. Croy, S. Mostafa, L. Hickman, H. Heinrich, B. Roldan Cuenya, *Applied Catalysis A-General* 350 (2008) 207–216.
- [40] S. Inamura, T. Hagashihara, Y. Saito, H. Aritani, H. Kanai, Y. Matsumura, N. Tsuda, *Catalysis Today* 50 (1999) 369–380.
- [41] M.P. Kapoor, A. Raj, Y. Matsumura, *Microporous and Mesoporous Materials* 44 (2001) 565–572.
- [42] Y.C. Lin, K.L. Hohn, S.M. Stagg-Williams, *Applied Catalysis A-General* 327 (2007) 164–172.
- [43] Y. Matsumura, W.J. Shen, *Topics in Catalysis* 22 (2003) 271–275.
- [44] B.E. Traxel, K.L. Hohl, *Applied Catalysis A-General* 244 (2003) 129–140.
- [45] R. Ubago-Perez, F. Carrasco-Marin, C. Moreno-Castilla, *Catalysis Today* 123 (2007) 158–163.
- [46] S. Mostafa, J.R. Croy, H. Heinrich, B.R. Cuenya, *Applied Catalysis A-General* 366 (2009) 353–362.
- [47] T. Iwasita, *Electrochimica Acta* 47 (2002) 3663–3674.
- [48] N.M. Markovic, P.N. Ross, *Surface Science Reports* 45 (2002) 121–230.
- [49] J. Christopher Brown, Erdogan Gulari, *Catalysis Communications* 5 (2004) 431–436.
- [50] T.P. Minyukova, I.I. Simentsova, A.V. Khasin, N.V. Shterstser, N.A. Baronskaya, A.A. Khassin, T.M. Yuriev, *Applied Catalysis A-General* 237 (2002) 171–180.
- [51] M. Mavrikakis, P. Stoltze, J. Norskov, *Catalysis Letters* 64 (2000) 101–106.
- [52] M. Valden, X. Lai, D.W. Goodman, *Science* 281 (1998) 1647–1650.
- [53] M. Haruta, *Catalysis Today* 36 (1997) 153–166.
- [54] S. Lambert, C. Cellier, F. Ferauque, E.M. Gaigneaux, B. Heinrichs, *Catalysis Communications* 8 (2007) 2032–2036.
- [55] Y. Matsumura, N. Tode, *Physical Chemistry Chemical Physics* 3 (2001) 1284–1288.
- [56] M. Mihaylov, T. Tsoncheva, K. Hadjiivanov, *Journal of Material Science* 46 (2011) 7144–7151.
- [57] T. Kim, M. Song, H. Koh, K. Kim, *Applied Catalysis A-General* 210 (2001) 35–44.
- [58] A. Corma, A. Palomares, F. Rey, F. Marquez, *Journal of Catalysis* 170 (1997) 140–149.
- [59] S. Kameoka, T. Tanabe, A. Tsai, *Catalysis Today* 93–95 (2004) 23–26.
- [60] T. Reitz, S. Ahmed, M. Krumpelt, H. Kung, *Journal of Molecular Catalysis A: Chemical* 162 (2000) 275–285.
- [61] M. Günter, T. Ressler, R. Jentoft, B. Bems, *Journal of Catalysis* 203 (2001) 133–149.
- [62] J. Agrell, M. Boutonnet, I. Meliañ-Cabrera, J.G. Fierro, *Applied Catalysis A-General* 253 (2003) 201–211.
- [63] M.E. Crivello, C.F. Perez, S.N. Mendieta, S.G. Casuscelli, G.A. Eimer, V.R. Elias, E.R. Herrero, *Catalysis Today* 133–135 (2008) 787–792.
- [64] M. Crivello, C. Perez, E. Herrero, G. Ghione, S. Casuscelli, E. Rodriguez-Castellon, *Catalysis Today* 107/108 (2005) 215–222.
- [65] S. El-Molla, *Applied Catalysis A-General* 298 (2006) 103–108.
- [66] R. Rioux, M. Vannice, *Journal of Catalysis* 233 (2005) 147–165.
- [67] V. Fridman, A. Davydov, K. Titievsky, *Journal of Catalysis* 222 (2004) 545–557.

- [68] F. Kovanda, K. Jirařová, J. Rymes, D. Kolousek, *Applied Clay Science* 18 (2001) 71–80.
- [69] R. Si, J. Raitano, N. Yi, L. Zhang, S.-W. Chan, M.F. Stephanopoulos, *Catalysis Today* (2011), <http://dx.doi.org/10.1016/j.cattod.2011.09.008>.
- [70] T. Montini, V. Gombac, L. Sordelli, J.J. Delgado, X. Chen, G. Adami, P. Fornasiero, *ChemCatChem* 3 (2011) 574–577.
- [71] E.S. Vasiliadou, A.A. Lemonidou, *Applied Catalysis A-General* 396 (2011) 177–185.
- [72] R.S. Rao, A.B. Walters, M.A. Vannice, *Journal of Physical Chemistry B* 109 (2005) 2086–2092.
- [73] S. Ruijuan, W. Fei, M. Xiaoling, T. Na, L. Yong, H. Xiumin, S. Wenjie, J. Chin., *Catalysis* 31 (2010) 626–630.
- [74] P. Serp, P. Kalck, *Chemical Reviews* 102 (2002) 3085–3128.
- [75] C. Vahlas, B. Caussat, P. Serp, G.N. Angelopoulos, *Materials Science and Engineering Reports* 53 (2006) 1–72.
- [76] X. Mu, U. Bartmann, M. Guraya, G.W. Busser, U. Weckenmann, R. Fischer, M. Muhler, *Applied Catalysis A-General* 248 (2003) 85–95.
- [77] W. Xia, D. Su, A. Birkner, L. Ruppel, Y. Wang, C. Wöll, J. Qian, C. Liang, G. Marginean, W. Brandl, M. Muhler, *Chemistry of Materials* 17 (2005) 5737–5742.
- [78] V. Dal Santo, C. Mondelli, V. De Grandi, A. Gallo, S. Recchia, L. Sordelli, R. Psaro, *Applied Catalysis A-General* 346 (2008) 126–133.
- [79] V. Dal Santo, A. Gallo, A. Naldoni, *Inorganica Chimica Acta* (2011), <http://dx.doi.org/10.1016/j.ica.2011.10.057>.
- [80] F.L.Y. Lam, A.C.K. Yip, X. Hu, *Industrial and Engineering Chemistry Research* 46 (2007) 3328–3333.
- [81] F.L.Y. Lam, X. Hu, *Chemical Engineering Science* 58 (2003) 687–695.
- [82] M. Becker, R.N. d'Alnoncourt, K. Kahler, J. Sekulic, R.A. Fischer, M. Muhler, *Chemical Vapor Deposition* 16 (2010) 85–92.
- [83] R.N. d'Alnoncourt, M. Becker, J. Sekulic, R.A.M. Fischer, M. Muhler, *Surface and Coatings Technology* 201 (2007) 9035–9040.
- [84] V. Dal Santo, A. Gallo, M.M. Gatti, V. De Grandi, R. Psaro, L. Sordelli, S. Recchia, *Journal of Materials Chemistry* 19 (2009) 9030–9037.
- [85] V. Dal Santo, C. Dossi, A. Fusi, R. Psaro, C. Mondelli, S. Recchia, *Talanta* 66 (2005) 674–682.
- [86] B. Veisz, Z. Kiraly, L. Toth, B. Pecz, *Chemistry of Materials* 14 (2002) 2882–2888.
- [87] G.S. Girolami, P.M. Jeffries, H. Dubois, *Journal of the American Chemical Society* 115 (1993) 1015–1024.
- [88] E.D. Guerreiro, O.F. Gorriz, G. Larsen, L.A. Arrúa, *Applied Catalysis A-General* 204 (2000) 33–48.
- [89] A.N. Pestryakov, V.P. Petranovskii, A. Kryazhov, O. Ozhereliev, N. Pfänder, A. Knop-Gericke, *Chemical Physics Letters* 385 (2004) 173–176.
- [90] A. Kong, H. Wang, X. Yang, Y.W. Hou, Y.K. Shan, *Microporous and Mesoporous Materials* 118 (2009) 348–353.
- [91] X. Lu, Y. Yuan, *Applied Catalysis A-General* 365 (2009) 180–186.
- [92] K.M. Parida, D. Rath, *Applied Catalysis A-General* 321 (2007) 101–108.
- [93] K. Hadjiivanov, G. Vayssilov, *Advances in Catalysis* 47 (2002) 307–511.
- [94] K. Hadjiivanov, T. Tsoneva, M. Dimitrov, C. Mintchev, H. Knözinger, *Applied Catalysis A-General* 241 (2003) 331–340.
- [95] G. Busca, U. Costantino, F. Marmottini, T. Montanari, P. Patrono, F. Pinzari, G. Ramis, *Applied Catalysis A-General* 310 (2006) 70–78.
- [96] N. Sheppard, T.T. Nguyen In: *Advances in Infrared and Raman Spectroscopy*, P.J. Clarke, R.E. Hester (eds.), Wiley, New York vol.5 (1978) 67–148.
- [97] M. Hartmann, S. Racouchot, C. Bischof, *Microporous and Mesoporous Materials* 27 (1999) 309–320.
- [98] X.-Y. Hao, Y.-Q. Zhang, J.-W. Wang, W. Zhou, C. Zhang, S. Liu, *Microporous and Mesoporous Materials* 88 (2006) 38–47.
- [99] L. Chmielarz, P. Kustrowski, R. Dziembaj, P. Cool, E.F. Vansant, *Microporous and Mesoporous Materials* 127 (2010) 133–141.
- [100] S.K. Reynolds, C.J. Smart, E.F. Baran, *Applied Physics Letters* 59 (1991) 2332–2334.
- [101] M.L.H. Heerdt, J.J.P. Overdijk, J. van der Put, J. Schoonman, *Chemistry of Materials* 11 (1999) 3470–3475.
- [102] M.L.H. ter Heerdt, P.J. van der Put, J. Schoonman, *Chemical Vapor Deposition* 7 (2001) 199–203.
- [103] S.L. Cohen, M. Liehr, S. Kasi, *Applied Physics Letters* 60 (1992) 50–52.
- [104] K. Hanaoka, K. Tachibana, H. Ohnishi, *Thin Solid Films* 262 (1995) 209–217.
- [105] K. Hanaoka, K. Tachibana, H. Ohnishi, *Thin Solid Films* 262 (1995) 209–217.
- [106] J.S. Mulley, R.A. Bennet, V.R. Dhanak, *Surface Science* 602 (2008) 2967–2974.
- [107] S.L. Cohen, M. Liehr, S. Kasi, *Applied Physics Letters* 60 (1992) 1585–1587.
- [108] S.L. Cohen, M. Liehr, S. Kasi, *Applied Physics Letters* 60 (1992) 50–52.
- [109] A. Gasparotto, D. Barreca, D. Bekermann, A. Devi, R.A. Fischer, P. Fornasiero, V. Gombac, O.I. Lebedev, C. Maccato, T. Montini, G. Van Tendeloo, E. Tondello, *Journal of the American Chemical Society* 133 (2011) 19362–19365.
- [110] Y.K. Chae, H. Komiya, *Journal of Applied Physics* 90 (2001) 3610–3613.
- [111] K. Hadjiivanov, E. Vassileva, M. Kantcheva, D. Klissurski, *Materials Chemistry and Physics* 28 (1991) 367–377.
- [112] N. Takezawa, N. Iwasa, *Catalysis Today* 36 (1997) 45–56.
- [113] I.A. Fisher, A.T. Bell, *Journal of Catalysis* 184 (1999) 357–376.